Journal of Nuclear Materials 457 (2015) 173–181

Contents lists available at ScienceDirect

Journal of Nuclear Materials

journal homepage: www.elsevier.com/locate/jnucmat

Hardening due to dislocation loop damage in RPV model alloys: Role of Mn segregation

D. Terentyev [a,*], X. He [b], G. Bonny [a], A. Bakaev [a,c,d], E. Zhurkin [d], L. Malerba [a]

[a] SCK·CEN, Nuclear Materials Science Institute, Boeretang 200, B-2400 Mol, Belgium
[b] China Institute of Atomic Energy, P.O. Box: 275-51, 102413 Beijing, China
[c] Center for Molecular Modeling, Department of Physics and Astronomy, Ghent University, Technologiepark 903, 9052 Zwijnaarde, Belgium
[d] Department of Experimental Nuclear Physics, Faculty of Physics and Mechanics, Institute of Physics, Nanotechnologies and Telecommunications, St. Petersburg State Polytechnical University, 29 Polytekhnicheskaya str., 195251 St. Petersburg, Russia

ARTICLE INFO

Article history:
Received 6 June 2014
Accepted 7 November 2014
Available online 14 November 2014

ABSTRACT

The exact nature of the radiation defects causing hardening in reactor vessel pressure steels at high doses is not yet clearly determined. While generally it is attributed to solute-rich clusters (precipitates) and point defects clusters (matrix damage), recent fine-scale experiments and atomistic simulations suggest that solute rich clusters, mainly containing Mn, Ni and Cu, might be the result of the segregation of these elements to small dislocation loops (heterogeneous nucleation), so that the distinction between precipitates and matrix damage becomes blurred. Here, we perform an atomistic study to investigate the interaction of $a_0/2\langle 1\,1\,1\rangle$ dislocation loops with moving dislocations and specifically address the effect of solute segregation on the loop's strength and interaction mechanism, focusing in particular on Mn, alone or with other crucial solute elements such as Cu and Ni. It is found that the enrichment of Mn in the core of dislocation loops causes significant increase of the unpinning stress, especially for small, invisible ones. At the same time, the solute segregation at the dislocation loops enhances their resistance against absorption by moving dislocations.

1. Introduction

Radiation-induced embrittlement of bainitic steels is the lifetime limiting factor of the reactor pressure vessels (RPV) in currently operating nuclear light water reactors (LWR). The primary mechanism of embrittlement is the obstruction of dislocation motion produced by nanometric defect structures that develop inside the material due to irradiation at the RPV operating temperature. Two classes of nano-structural features are considered to contribute to the embrittlement of RPV steels, both hardly detectable by means of transmission electron microscopy (TEM). These are (i) clusters of Cu, Ni, Mn and other solutes, generally catalogued as *precipitates*; and (ii) the so-called *matrix damage*, interpreted as clustering of point-defects [1–4]. The former features are further subdivided into Cu-rich precipitates (CRP), which have been long identified as an important source of hardening [1], and Mn–Ni-rich precipitates (MNP). The latter are expected to contribute significantly to hardening especially in low-Cu/high-Ni steels (i.e. Cu << 0.1 wt%, Ni > ~1 wt.%) and for relatively low irradiation temperatures, within the narrow range of RPV operating temperatures depending on the reactor (265–290 °C) [2]. They are therefore proposed to explain the increase of hardening at high dose (i.e. beyond 0.1 dpa) [5] that is not reflected in existing trend curves. Due to the 'late' (in terms of irradiation dose) appearance of these nano-features, and assuming they are stable thermodynamic phases that might suddenly develop in large volume fractions, they are often called 'late blooming phases' (LBP) [2,5]. Based on a combination of experimental observations and atomistic studies, they are currently understood as radiation-induced agglomerations of Mn–Ni-rich clusters on point-defect clusters [6–8], thereby making the distinction between precipitates and matrix damage somewhat ambiguous.

Nanovoids and vacancy-solute clusters, together with Cu precipitates, were initially identified as the main source of hardening

Abbreviations: RPV, reactor pressure vessel; LWR, light water reactor; TEM, transmission electron microscopy; CRP, copper rich precipitates; MNP, Manganese–Nickel precipitates; PAS, positron annihilation spectroscopy; MD, molecular dynamics; DL, dislocation loop; PWR, pressurized water reactor; MMC, Metropolis Monte Carlo; BV, Burgers vector; DGP, dislocation glide plane; CS/TS, compression/tension site; RM, reaction mechanism; RSS, resolved shear stress.

* Corresponding author. Tel.: +32 14 333197; fax: +32 14 321216.
E-mail address: dterenty@sckcen.be (D. Terentyev).

http://dx.doi.org/10.1016/j.jnucmat.2014.11.023
0022-3115/

in RPV steels [1]. However, positron annihilation spectroscopy (PAS) studies do not reveal the formation of nanovoids in RPV steels irradiated under conditions of technological relevance: only small clusters containing a few vacancies are found [7,9,10]. In Fe–Cu model alloys these are deduced by PAS to be associated with Cu-rich precipitates [10,11]. Dedicated atomistic molecular dynamics (MD) studies of the interaction of dislocations with Cu-vacancy-rich precipitates suggest, however, that, while full Cu precipitates may partially contribute to RPV steel hardening, the contribution of solute–vacancy-type defects to hardening is doubtful [12,13].

Nanometric dislocation loops (DL), typically observed in bcc Fe and Fe-based RPV-model alloys at relevant irradiation conditions [7], offer an alternative explanation for the hardening. TEM observation of fairly small (<5 nm in diameter) DLs has been reported in Russian-type VVER steels [14–17], although generally not in "Western-type" pressurized water reactor (PWR) steels [7,18,19]. However, higher irradiation doses with ions or electrons make interstitial-type dislocation loops visible also in typical PWR steels [20,21]. Moreover, recent accurate studies revealed the presence of low densities ($\sim 10^{20}$ m^{-3}) of small DL, often decorating dislocations and grain boundaries, also in neutron-irradiated RPV steels from surveillance specimens of European nuclear power plants. It is therefore reasonable to assume that DLs are indeed always present in irradiated RPV steels, but remain too small to be easily detected by TEM up to irradiation doses typical for RPV end of life. The recent indications that these small loops might be decorated by solute atoms (Mn, Ni, Cu, etc.) which would find there the appropriate location to precipitate even outside the range of thermodynamic stability of phase separation [6], suggest that small loops and especially solute-decorated small loops should be studied as possible source of radiation hardening in RPV steels.

In this work, we perform MD simulations to investigate the interaction of DLs with moving dislocations using the configurations of the interstitial loops decorated by Mn, Ni and Cu atoms obtained from a preceding simulation study, using Metropolis Monte Carlo (MMC) techniques with an appropriate interatomic potential [6]. While in pure Fe the majority of loops are of $\langle 1\,0\,0\rangle$ type [19], both types of loops with Burgers vector (BV) $a_0/2\langle 1\,1\,1\rangle$ and $a_0\langle 1\,0\,0\rangle$ are present in RPV steels [21] and model Fe-based alloys containing Mn, Ni and Cu [7,22,23]. Since $a_0/2\langle 1\,1\,1\rangle$ loops are primarily seen in displacement cascades in bcc Fe [24,25] irrespective of the applied interatomic potentials [26], we begin our investigation considering these DLs. Given that the DLs of concern in RPV steels are believed to be at the limit of the TEM resolution, we consider relatively small defects, 1.5, 3.5 and 5 nm in diameter, interacting with an edge dislocation at room temperature (test temperature). The effect of solute enrichment on the strength with which the obstacle opposes to dislocation movement is studied in the binary Fe–Mn, ternary Fe–Mn–Ni and quaternary Fe–Mn–Ni–Cu systems. As a first step, the main accent is put on the effect of Mn as this element is known to exhibit strong interaction with both vacancies and self-interstitial atoms [27], so its segregation to dislocation loops is primarily expected.

2. Computational details

To perform MMC and molecular dynamics (MD) simulations we describe the atomic interaction in the Fe–Mn–Ni–Cu system applying the interatomic potential developed by Bonny et al. in [6]. The potential was developed accounting for point-defect solute interactions as well as thermodynamic consistency with experimental phase diagrams. The pure elements: Fe, Mn, Ni and Cu were taken from Refs. [28,6,29] and [30], respectively. The cross potentials for FeMn, NiMn and CuMn were fitted in [6], NiCu in [31], FeNi in [32] and FeCu in [33].

2.1. DL configurations for MD simulations

The equilibrium arrangements of Mn, Ni and Cu atoms around $a_0/2\langle 1\,1\,1\rangle$ circular DLs are obtained by using MMC sampling [34] within the isobaric grand canonical ensemble (NPT), where number of particles (N), pressure (P) and temperature (T) are preserved. The method includes three sequential types of trials to make the system evolve from a given initial condition to equilibrium: (i) a random displacement of all atoms from their current positions (by this trial, lattice relaxation and vibrational entropy are accounted for); (ii) the overall volume change of the simulation box (this trial allows the desired pressure to be maintained, even if a structural transition were to occur); (iii) the third trial consists in the random exchange of two atoms of different species (by this trial the equilibrium configurations are sampled). The decision on the acceptance of the new configuration is based on the standard MMC algorithm [34] and one set of these trials is termed an "MC step". The convergence of the total energy usually required about 5×10^6 MC steps (starting from the random crystals pre-thermalized by MD simulations) for crystals containing $\sim 22 \times 10^3$atoms, i.e. sufficiently large to avoid loop self-interaction via periodic boundary conditions.

As mentioned in the introduction focus here is made on the effect of Mn, including the case of presence of also other solutes. We therefore consider the following alloys at 600 K: Fe–0.5%Mn, Fe–1%Mn, Fe–2%Mn, Fe–1%Ni–1%Mn, Fe–2%Mn–2%Ni and Fe–0.8%Mn–0.8%Ni–0.5%Cu. As an example of the results of MMC simulations performed in $6.3 \times 6.3 \times 6.3$ nm^3 crystal, Fig. 1 provides a visualization of the MnNiCu precipitate formed near a 3.5 nm hexagonal $a_0/2\langle 1\,1\,1\rangle$ interstitial loop (containing about 170 self-interstitial defects) in the Fe–0.8%Mn–0.8%Ni–0.5%Cu system equilibrated at 600 K. The equilibrated MMC crystals were then embedded in a larger MD sample that contained a pre-relaxed dislocation. The MD crystal was relaxed again, thermalised at the desired test temperature (e.g. 300 K) and finally loaded to induce the DL-dislocation interaction. Details of the MD simulations are provided in the following subsection.

In this work, we investigate how the equilibrium solute rearrangement in the core of DLs affects the DL-dislocation interaction mechanism and critical unpinning stress. While the solute re-distribution around the loop was obtained via MMC simulations similar to [8], the analysis was here made in a different way.

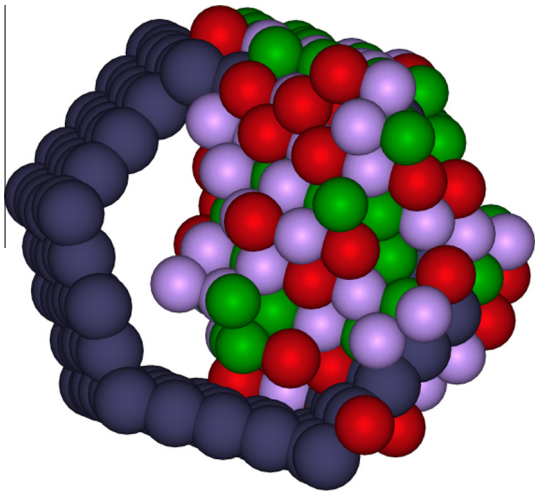

Fig. 1. Arrangement of Mn, Ni and Cu atoms in a MnNiCu precipitate formed on a $a_0/2\langle 1\,1\,1\rangle$ DL. Mn, Ni and Cu are shown by purple, red and green spheres, respectively, while dark blue spheres indicate atoms constituting the core of the DL. (For interpretation of the references to colour in this figure legend, the reader is referred to the web version of this article.)

Namely as a measure of the solute re-arrangement we searched for the chemical types of the atoms constituting the loop core and those present in the immediate vicinity i.e. in the nearest compressed and tensile shells (see [35] for a more detailed description). Even though some solute clusters (precipitates) whose size exceeds these regions of the loop might form after MMC simulations, depending on initial alloy composition and loop size (Fig. 1 is an example), we neglect their presence, as here we exclusively investigate the effects attributed to the solute enrichment in the core of DLs. The present approximation is based on the idea that the core atoms of a DL contribute mainly to the interaction with a dislocation and its obstacle strength with respect to the dislocation passage. The impact of solute precipitation on dislocation loops will be the subject of a separate study.

2.2. MD simulations

To study dislocation–loop interaction we employed the simulation algorithm developed by Osetsky and Bacon [36]. In this study, we considered the {110} slip system, which is the primary slip system in BCC lattice [37], and the edge dislocation, which is known to be especially efficient in direct absorption of dislocation loops [38]. The principal axes x, y and z of MD crystal, shown in Fig. 2, were oriented along the [1 1 1], [$\bar{1}\,\bar{1}$ 2] and [1 $\bar{1}$ 0] orthogonal directions, respectively, so that periodic conditions could be applied along the dislocation glide plane and dislocation line. The edge dislocation with BV = $a_0/2\langle 1\,1\,1\rangle$ in the $(1\,\bar{1}\,0)$ slip was created along the y direction. Periodic boundary conditions were applied along the x and y directions. Along z, the box was divided into three parts: the upper and lower parts consisted of several atomic planes in which atoms were rigidly fixed in their original position relative to each other, whereas atoms in the inner region were free to move during the MD runs, thus responding to the externally applied shear. The latter was generated by displacing the upper rigid block in the x direction, which corresponds to applying simple shear strain e_{xz}. Correspondingly, the shear strain resulted in a glide force on the dislocation. The corresponding resolved shear stress induced by the applied deformation was calculated as $\sigma_{zx} = F_x/A_{xy}$, where F_x is the total force in the x direction on the lower rigid block due to the atoms in the inner region, and A_{xy} is the xy cross-section area of the box. The size of the inner region of the MD box was 101×3, 30×6 and 25×2 non-equivalent atomic planes along x, y and z (or $25 \times 21 \times 10$ nm^3), respectively, and it contains around 450 thousands atoms. Such crystallite is large enough to consider the interaction of the dislocation with a loop of diameter up to 5 nm (350 self-interstitial atoms, SIAs), as shown in our previous studies [39–41]. During an MD run, the dislocation line and loop were monitored using atomic disregistry analysis, coupled with structural nearest-neighbour analysis (see [42]), as well as by selecting atoms with high potential energy. Statistical averaging

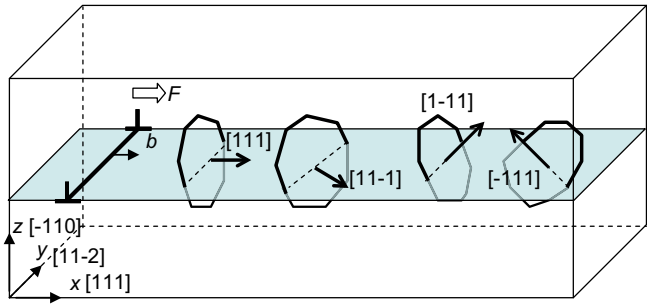

Fig. 2. Interaction geometry for four possible orientations of $a_0/2\langle 1\,1\,1\rangle$ loops interacting with an edge dislocation with BV = $a_0/2[1\,1\,1]$. F denotes the direction of the shear force that acts on the dislocation.

was performed every 250 steps to reveal the atoms belonging to the dislocation core. The latter procedure allowed the identification of the interaction mechanism even at relatively high temperature, despite the significant thermal noise.

MD simulations were started by initializing the velocity of the relaxed atoms according to the Maxwell's distribution for the desired simulation (mechanical test) temperature, T, chosen to be in the range of 150–800 K. After thermalization for 10^3 steps, load was applied at a fixed strain rate, resulting in a dislocation velocity (v_d) of 10 m/s. A relatively high dislocation velocity, typically in the range 0.1–100 m/s, is an intrinsic caveat of MD simulations limited to the timescale of nano-seconds. To achieve the desired v_d, the strain rate to be applied, $\dot{\varepsilon}$, was determined according to Orowan's law $\dot{\varepsilon} = pbv_d$, where p is the dislocation density, equal to $1/(L_X \times L_Z)$ and b is the BV. The integration of Newton's equations was performed using a constant time-step (2.5 fs) in the microcanonical NVE ensemble, in which number of particles, system volume and total energy (E) are conserved if the work of external forces is taken into account. No temperature control was applied to limit temperature increase during the simulation, but the latter was always negligible.

3. Results

3.1. Reference interaction mechanisms and loop's strength

Prior to describing the effect of solute segregation, we recall the interaction mechanism and strengthening of $a_0/2\langle 1\,1\,1\rangle$ loops in pure Fe, under the loading conditions applied here. Two out of four possible interaction geometries, shown in Fig. 2, namely: $\boldsymbol{b}_L = a_0/2[\bar{1}\,1\,1]$ and $a_0/2[1\,\bar{1}\,1]$, represent the case when the BV is inclined with respect to the dislocation glide plane (DGP). In the other two cases the BVs of the loops are parallel to the DGP and these can therefore be dynamically dragged or pulled by the approaching dislocations. The latter interaction causes very little or no resistance to the dislocation glide, because the migration energy of $a_0/2\langle 1\,1\,1\rangle$ loops is very small (0.05 eV) so its glide is practically an athermal process [43]. The case of the loop with BV = $1/2[11\bar{1}]$ intersecting the glide plane has been recently studied in [44]. It was shown that the loop can also be dragged by the dislocation although at significantly lower dislocation velocity. The dislocation and loop enter the reaction forming a configuration that contains two 'quadra-point' junctions, see Fig. A1(b) in Ref. [44]. This junction is hardly mobile and therefore its stability determines the critical breakaway stress, while its mobility defines the condition for dynamic drag. Given the applied loading conditions and for the loop sizes studied here, the dynamic drag does not occur and the loop is eventually sheared by the dislocation once a significant shear stress is reached (which is ~250 MPa at 300 K for a 3.5 nm loop).

The resistance of the loops with the BV inclined to the DGP is much higher than in the case of dynamic drag. The interaction mechanism requires the formation and propagation of a reaction segment of $\langle 1\,0\,0\rangle$ type. Both inclined configurations have already been thoroughly studied in bcc Fe in [38,45,46] and, for the loading conditions applied here, the expected critical stress for 1.5, 3.5 and 5 nm loops at 300 K is 50, 300 and 360 MPa, respectively.

3.2. Local solute arrangement around dislocation loops

In the alloys studied here, the decoration of solutes was seen on both compression (CS) and tensile sites (TS) of the loop core in approximately equal amounts. Here, as in our previous MMC study carried out in Fe–Cr alloys [47], the enrichment (x_{sol}) is quantified as concentration of solutes among the atoms belonging to the dis-

Table 1
Solute composition in the 3.5 nm DL core after MMC calculations.

Alloy's composition	$x_{sol\ (CS)}$	$x_{sol\ (TS)}$	x_{sol}
0.5%Mn	Mn = 7%	Mn = 9%	Mn = 8%
1%Mn	Mn = 18%	Mn = 20%	Mn = 19%
2%Mn	Mn = 32%	Mn = 37%	Mn = 34%
1%Mn–1%Ni	Mn = 15% Ni = 7%	Mn = 19% Ni = 8%	Mn = 17% Ni = 7.5%
2%Mn–2%Ni	Mn = 22% Ni = 6%	Mn = 26% Ni = 6%	Mn = 24% Ni = 6%
0.8%Mn–0.8%Ni–0.5%Cu	Mn = 19% Ni = 10% Cu = 1%	Mn = 22% Ni = 10% Cu = 1%	Mn = 21% Ni = 10% Cu = 1%

location loop core, defined using the structural analysis. In the Fe–Mn binary alloys, $x_{sol\ (CS)}$ was always about 10% lower than $x_{sol\ (TS)}$. Both values grow approximately linearly with increasing Mn content in the matrix. With addition of Ni, some Mn atoms were replaced by Ni and Fe atoms, so the solute content in the loop core in Fe–1%Mn–1%Ni became lower than $x_{sol\ (CS\ or\ TS)}$ in Fe–2%Mn. The content of Ni decorating the loop was about three times lower than that of Mn in Fe–1%Mn–1%Ni, and four times lower in Fe–2%Mn–2%Ni. In the quaternary alloy, the Mn content in the core was 20%, with 0.110% Ni and 1% Cu. Despite very weak Cu segregation, the addition of Cu recovers Mn segregation and enhances segregation of Ni, as compared to the local atomic arrangement found in the ternary Fe–Mn–Ni system. The solute decoration is not spread over the whole loop perimeter homogeneously in all the cases and sometimes is seen to be localized.

The average concentration of the solutes in the compression and tensile sites of the 3.5 nm DL core is reported in Table 1. The trends observed in the enrichments computed for 1.5 and 5 nm loops were similar to those discussed above. More details about the deposition of Mn, Ni and Cu in binary, ternary and quaternary alloys can be found in [8].

3.3. Interaction of enriched loops with dislocations

In the simulations employing MMC-obtained DL configurations, four different reaction mechanisms (RM) were distinguished. Their brief description is as follows:

(i) Complete removal of the loop, which occurs by its incorporation on the dislocation line or by dynamic drag.
(ii) Partial absorption i.e. reduction of the loop size without modification of its orientation, which occurs when the absorption reaction started but did not get to completion (see examples of the interaction with inclined loops at low temperature [41]). Another reaction pathway was identified in the reactions involving loops with BV = $a_0/2[1\,1\,1]$ immobilized by the solute decoration, the examples will follow.
(iii) Loop shear, which was seen only for DLs with BV = $a_0/2[1\,1\,-1]$: while in the case of undecorated loops $\langle 0\,0\,1\rangle$ type junctions with limited mobility formed on contact, here the loops remain completely immobilized by the solute decoration.
(iv) Orowan-type reaction, which corresponds to the case when the loop opposes strong resistance to the dislocation. At sufficiently high shear stress, the emergence of a screw dipole and its closure occurs at resolved stress close to the Orowan limit (i.e. $\mu b/L$, where μ and L is the shear modulus and free dislocation passage distance, respectively).

Strong impact of solute segregation on the critical stress is found only for 1.5 nm DLs. The suppression of loop absorption, promoted by the segregation of Mn, was observed for larger loops, as will be shown in the following examples.

Our first example refers to the interaction of solute-enriched loops with BVs contained in the DGP. Consider the stress–strain relationship shown in Fig. 3(a) corresponding to the interaction of the dislocation with a 3.5 nm $a_0/2[1\,1\,1]$ loop, whose equilibrium configuration was obtained in the Fe–1%Mn alloy (so, it contains ~20% Mn atoms in the core region). In this interaction geometry, the undecorated loop (pure Fe in the figure) simply glides in front of the approaching dislocation, under the action of the repulsive force. The steady-state stress for the applied loading conditions (i.e. loop size and temperature) is only ~20 MPa, i.e. very low. The visualization of the interaction process for the decorated loop is given in Fig. 4. One sees that, being decorated, the loop does not glide at all: the resolved shear stress (RSS) keeps increasing and, as the dislocation approaches, a local backward bending of the dislocation line is clearly produced (see Fig. 4(b)). Once the RSS reaches 70 MPa, the dislocation overcomes the repulsive interaction and makes contact with the loop (see Fig. 4(c)), determining a drop in

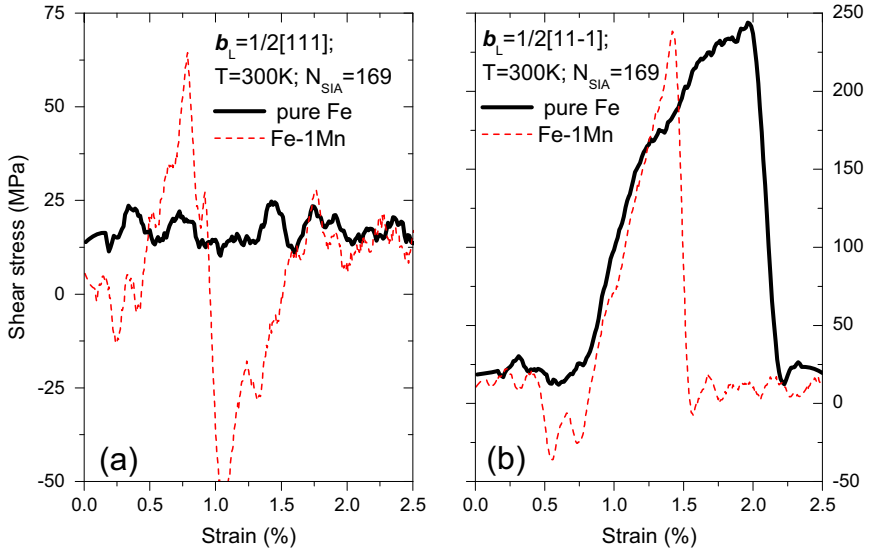

Fig. 3. Stress–strain relationship corresponding to the interaction of 3.5 nm DLs with (a) BV = $a_0/2[1\,1\,1]$ and (b) BV = $a_0/2[1\,1\,-1]$.

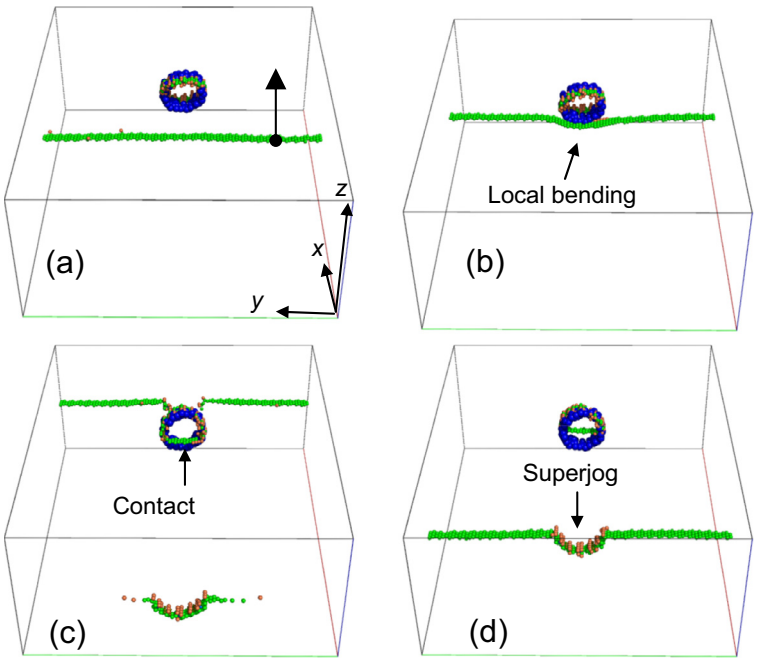

Fig. 4. Visualization of the interaction of an edge dislocation with Mn-decorated $a_0/2[-1\,1\,1]$ DL of size 3.5 nm, modelled at 300 K. The equilibrium arrangement of Mn solutes (shown by blue balls) is obtained after MMC simulations in Fe–1%Mn alloy. (For interpretation of the references to colour in this figure legend, the reader is referred to the web version of this article.)

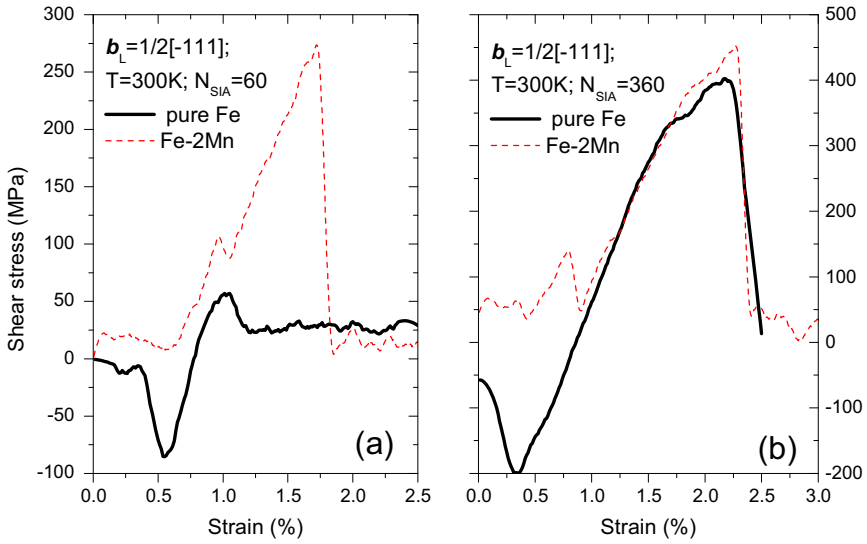

Fig. 5. Stress–strain relationship corresponding to the interaction of $a_0/2[-1\,1\,1]$ DLs of size (a) 1.5 nm and (b) 5 nm.

the RSS which, in fact, becomes negative as a consequence of the reaction. The result (see Fig. 4(d)) is that the lower part of the loop is absorbed on the dislocation line as a superjog, while the upper part remains attached to the decorating Mn atoms, which remain in their original positions.

The stress–strain curve for another interaction geometry with BV contained in the DGP is shown in Fig. 3(b). In this case, we see that the profiles of the stress rapidly increase with strain both for the decorated and undecorated loop. However, for the former the growth is practically linear, which implies that almost no plastic deformation occurs before the dislocation unpins from the loop. This is the main effect of solute segregation in this case which, for the rest, hardly influences the RSS maximum value. However, in terms of the details of the interaction mechanism the difference is important. Let us recall the process for the undecorated loop, illustrated graphically in Ref. [44]. As the dislocation contacts the loop, there is the formation of a new configuration containing two [001] nodes. These act as a bridge connecting $1/2[1\,1\,1]$ and $1/2[1\,1\,\bar{1}]$ segments cutting each other. For some time the whole complex is stable, but once the RSS reaches ~175 MPa, the loop-dislocation configuration begins to move. The loop displaces along the dislocation line (in the $[1\,1\,-1]$ direction) while the latter advances. This movement occurs via a mechanism that involves break-up and reconstruction of the [001] junctions. The latter therefore controls the critical stress at which this configuration glides as a whole. Break-up or stable drag are therefore determined

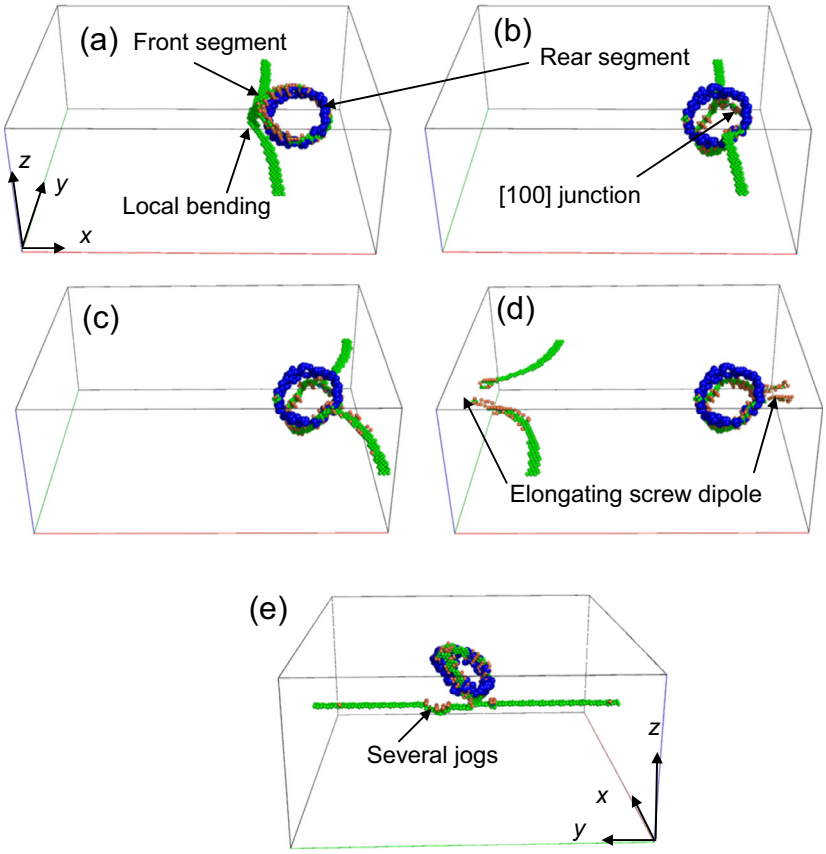

Fig. 6. Visualization of the interaction of an edge dislocation with $a_0/2[-1\,1\,1]$ DL of size 5 nm modelled at 300 K. The equilibrium arrangement of Mn solutes (shown by blue balls) is obtained after MMC simulations in Fe–1%Mn alloy. (For interpretation of the references to colour in this figure legend, the reader is referred to the web version of this article.)

by deformation speed and temperature (needed to activate break-up of [0 0 1] junctions). In the applied conditions, the deformation speed is too high to see stable glide and the loop is finally sheared at the critical stress of ~250 MPa. The evidence for the limited drag (and plastic deformation) is seen on the stress–strain curve as an increase from the straight line, which is not observed for the decorated loop (loaded in the same conditions). Visual inspection has proven that the decorated loop was completely immobilized by the solutes and no displacement along the dislocation line was observed in this case.

Our next example demonstrates the strong effect that enrichment may have also on the unpinning stress, while the reaction mechanism proceeds in the same way. Consider the stress–strain relationship shown in Fig. 5(a), that corresponds to the interaction of a 1.5 nm loop with BV = $a_0/2[-1\,1\,1]$. This is the case of the inclined configuration, previously studied by several independent researches [38]. It is well established that, for loops with size below 2 nm, the inclined interaction in pure Fe results in the complete absorption of the loop by its flip and incorporation on the dislocation line in the form of a superjog. The critical stress of 50 MPa (see Fig. 5(a)) is only needed to reform the superjog into a glissile configuration. The decorated loop opposes much stronger resistance to this process, even though eventually it is completely absorbed by the dislocation. Note that the RSS does not become negative as the dislocation approaches the decorated loop. This occurs because the loop was completely immobilized by Mn atoms, so that it did not glide in its prism to establish the optimum interaction geometry. Overcoming the initially repulsive interaction, the dislocation makes eventually contact also with the decorated loop and forms the mixed [1 0 0] reaction segment, which propagates along the loop surface once the RSS reaches 275 MPa. So, the solute enrichment turns out to change the interaction mechanism (though not the reaction outcome), leading to a major increase of the unpinning stress, by approximately a factor five. As will be shown later, the effect of the enrichment is inherently dependent on the Mn content in the loop core, specifically for this interaction geometry and loop size.

The evolution of stress–strain relationships for a larger, 5 nm size, loop in the same interaction geometry is presented in Fig. 5(b). In this case the unpinning stress is close to 400 MPa for both undecorated and enriched loops. Nevertheless, there is an important effect of solute enrichment on the reaction outcome. While the undecorated loop is completely absorbed (see Section 3.1), the enrichment almost totally suppresses the absorption. Let us consider the details of the interaction mechanism, presented in Fig. 6. The dislocation approaches the loop and bends backwards due to the repulsion from the front loop segment (Fig. 6a). The repulsive interaction displaces the front loop segment above the dislocation glide plane and the dislocation comes into contact with the rear loop segment to form the reaction segment with ⟨0 0 1⟩ orientation (Fig. 6b). The latter pins the dislocation (Fig. 6c) and eventually a screw dipole emerges (Fig. 6d). The dipole closes by the glide of the two arms (with a couple of cross-slip events), resulting in the breakaway of the dislocation and restoration of the loop in its original position (Fig. 6e). This effect points to a very important implication with respect to the transfer of these results to DD techniques, as local chemical arrangement becomes another variable defining the reaction outcome. Another implication is that by suppressing absorption the damaged matrix remains hard to the passage of new dislocations and the formation of defect-free channels is prevented or, at least, delayed.

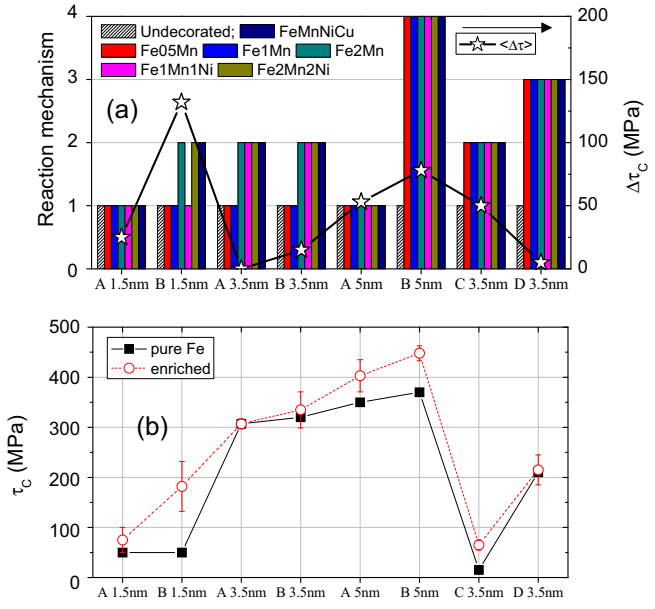

Fig. 7. (a) Interaction mechanism (left *Y* axis) and added critical resolved shear stress (right *Y* axis) as functions of loop size and its Burgers vector. (b) Unpinning stress for the undecorated and the averaged unpinning stress (averaged over the six different chemical configurations) for the enriched loops. Letters 'A', 'B', 'C', and 'D' on *X* axes refer to the orientation of Burgers vector of the DLs as [1 −1 1], [−1 1 1], [1 1 1] and [1 1 −1], respectively. The numbers on *Y* axis in (a) refers to the following interaction mechanisms: (1) absorption/drag; (2) partial absorption/replacement; (3) shear, (4) Orowan-like reaction, see description of the mechanisms in text.

3.4. Summary and discussion

Fig. 7 summarizes the main results of this work. Fig. 7(a) shows graphically the types of interaction mechanisms as functions of loop size and configuration. One can see that a systematic change in the interaction mechanism takes place for the loops with BV = $a_0/2[-1\,1\,1]$, irrespective of the loop size. The interaction mechanism is also different for the loops with BVs contained in the DGP, irrespective of the type of solute enrichment. Finally, the interaction mechanism remains unchanged in the two interaction geometries involving the $a_0/2[1\,-1\,1]$ loops with size 1.5 and 3.5 nm.

The unpinning stress for the undecorated and enriched loops is compared in Fig. 7(b). In the case of the decorated loops, we consider the mean value defined by averaging over the six different chemical configurations considered. One can see that the averaged unpinning stress for the enriched loops is higher or similar to the one in pure Fe. The increase of the unpinning stress is superimposed in Fig. 7(a), showing some correlation with the modification of the interaction mechanism in the case of $a_0/2[-1\,1\,1]$ loop. However, it is to be mentioned that the relative increase of the stress (i.e. $\tau_{enriched}/\tau_{undecorated}$) depends strongly on loop size. In the case of the $a_0/2[-1\,1\,1]$ loop, it is 5 and 1.2, respectively for 1.5 and 3.5 nm.

One must also note the relatively large spread of the mean value of the unpinning stress for the 1.5 nm loop, see Fig. 7(b). A detailed comparison of the loading curves in all inspected configurations is presented in Fig. 8(a). The unpinning stress clearly correlates with the Mn content in the loop core, thereby demonstrating the importance of the segregation of Mn specifically. It is worth noticing that Mn exhibits very strong attractive interaction with a ⟨1 1 1⟩ crowdion i.e. −0.75 eV, while Ni and Cu are nearly neutral [27]. Cr atoms are also attracted to the ⟨1 1 1⟩ crowdion with the interaction of −0.4 eV, which is almost twice as low. Since the DL-dislocation reaction involves the re-orientation of crowdions forming the loop core, the strong solute–crowdion interaction suppresses the dislocation reaction. The significant affinity of Mn to ⟨1 1 1⟩ crowdions (adequately captured by the interatomic potential used) may explain why the content of Mn in the loop core defines its resistance to the dislocation passage. The segregation-induced suppression of the loop re-orientation may also take place for solutes segregating to the tensile core region, which would translate to the compressed region after the loop reorientation. In this case, the repulsive interaction with ⟨1 1 1⟩ crowdions would be equivalent resisting force suppressing DL-dislocation reaction. Hence, the ability of segregating solutes to suppress the reaction with dislocations should depend not on the sign of the interaction but on its absolute strength.

To demonstrate this let us compare the effect of segregation of Mn and Cr. For the latter, we consider the results obtained for the 1.5 nm loop equilibrated by MMC in Fe–10%Cr at 600 K from [44] ($x_{sol} \sim 0.2$ i.e. comparable to the enrichment obtained in the Fe–1%Mn alloy). Clearly, the Cr enrichment of small loops has much weaker effect on the unpinning stress as compared to the Mn enrichment, which is consistent with the much stronger affinity of Mn to the ⟨1 1 1⟩ crowdion. To make this statement even more robust, we provide in Fig. 8(b) the results preliminarily obtained for 3 nm size $a_0\langle 0\,1\,0\rangle$ loops, whose configurations were prepared by equivalent MMC runs as for $a_0/2\langle 1\,1\,1\rangle$ loops. We obtained essentially the same trends as in the case of $a_0/2\langle 1\,1\,1\rangle$ loops, namely: (i) Mn enrichment enhances loop's strength; (ii) Mn decoration has much stronger effect than Cr; however, in this case the

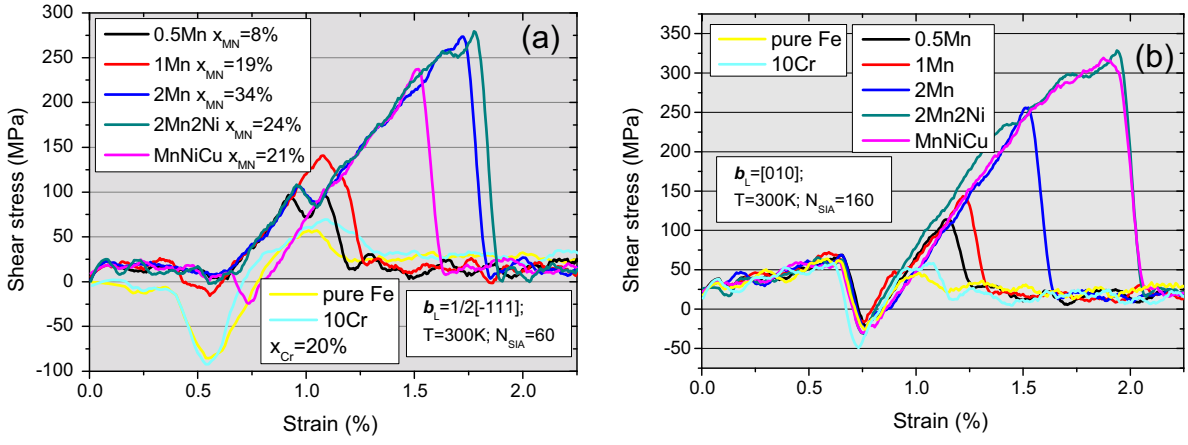

Fig. 8. Stress–strain relationship corresponding to the interaction of (a) $a_0/2[-1\,1\,1]$ DLs of size 1.5 nm and (b) $a_0[0\,1\,0]$ DLs of size 3.5 nm, whose configurations were obtained by MMC simulations in several alloys. The composition of the alloys is reported in the figure inset, as well the concentration of Mn in the loop core.

presence of Ni seems to be more determinant than the presence of Mn, possibly because of the type of interaction between Ni and ⟨100⟩ crowdions. Detailed investigation of the enrichment on ⟨100⟩ loops will be given in our upcoming work.

The observations discussed above bring us to the important conclusion that loop-dislocation interaction depends not only on the degree of segregation (i.e. content of solutes in the loop core), but also on the strength of the specific solute–loop interaction. The segregation of Cu or Ni or Mn on a given loop is not equivalent. Among Mn, Ni and Cu, the first element seems to have the strongest effect, although the effect of Ni in the binary alloy still needs to be investigated. At the same time, the analysis of the MMC data discussed in Section 3.2, suggests competitive interaction between Mn, Ni and Cu. The addition of Ni to a ternary Fe–Mn–Ni alloy weakens Mn segregation, while the addition of Cu in the quaternary Fe–Mn–Ni–Cu alloy reduces Ni segregation at loops and consequently enhances Mn content in the loop core. Thus, small variations of Mn, Ni, Cu concentrations dissolved in the matrix may lead to a significant change in the chemical potential for Mn segregation at loops, thereby influencing also the degree of radiation hardening. Another issue not to be forgotten is the complementary decoration of loops by carbon atoms. Even though dissolved in small amounts, carbon has enormous influence on the loop mobility and on the interaction with dislocations [35,48]. Given that Mn is known to enter carbides and substitutional Mn exhibits attractive interaction with interstitial carbon in bcc Fe [49], the synergic Mn–C interaction on the dislocation loop core should have strong contribution to the establishment of the local chemistry and even further on the resulting hardening.

In RPV steels, the decoration of dislocation loops by solutes occurs under continuous neutron irradiation at ~300 °C. On the one hand, the solutes will be transported by radiation induced defects, which obviously have different mass transport efficiency. The latter will depend on the concentration of solutes dissolved in the matrix, on temperature, and also on local solute–defect interactions. Depending on the efficiency of each transport mechanism, the fluxes of solutes and defects reaching dislocation loops will change: these are kinetic factors that will influence the local chemistry around loops. On the other hand, thermodynamics will also play a role to determine the type of phase that should eventually precipitate on the loops at steady state, if not equilibrium. This will also be influenced by the competition with other stable phases. For example the concentration of solutes dissolved in matrix will be influenced also by the formation of CRP that will likely contain also vacancies, the presence of which has been undoubtedly confirmed by several experimental techniques. Hence, the precise determination of the local chemistry around small dislocation loops that are barely visible by TEM and not recognizable by other techniques remains a difficult task both for atomistic simulations and experiments. It seems therefore reasonable to envisage limiting cases for solute segregation at dislocation loops, to be validated using refined advanced experimental techniques (e.g. atom probe), and apply atomistic simulations to evaluate the consequences with regard to plastic deformation.

4. Conclusions

Based on the above results and discussion, we can summarize as follows our conclusions:

1. In Fe–Mn binary, Fe–Mn–Ni ternary and Fe–Mn–Ni–Cu quaternary alloys the segregation of Mn to the core of $a_0/2\langle 111\rangle$ dislocation loops occurs at equilibrium at 600 K. When analyzing the regions close to the dislocation loop core, Mn appears to be the most strongly segregating element, while Cu is the weakest one. Mn and Ni occupy competing positions in the loop core, so the segregation level of Mn in the ternary alloy is lower than in the binary. At the same time, the addition of Cu suppresses the segregation of Ni, so that Mn concentration in the loop core recovers back, as a result. Hence, the interplay between all three chemical elements will contribute to the final chemical arrangement (without accounting for kinetic effects). In any case, Mn seems to always prevail, its content being about 2–3 and 5 times higher than that of Ni and Cu, respectively. Mn is therefore expected to play the major role on the properties of loops upon plastic deformation in the quaternary Fe–Mn–Ni–Cu alloys. The separate effect of the other elements, however, still needs to be assessed.
2. The study of the interaction with edge dislocations of small, 1.5 nm diameter $a_0/2\langle 111\rangle$ dislocation loops enriched with Mn, Mn–Ni and Mn–Ni–Cu reveals that the main effect of the enrichment is the significant increase of the unpinning stress, especially in small loops. By increasing Mn content in the core of the loops, the unpinning stress increases too. This effect has obviously direct consequences on increasing the radiation hardening attributed to the so-called matrix damage.
3. The study of the interaction with edge dislocation of larger (3.5 and 5 nm diameter) $a_0/2\langle 111\rangle$ loops reveals that the enrichment suppresses mainly the absorption and dynamic drag of loops i.e. reactions involving instantaneous removal of loops by the dislocation front. Instead of being absorbed, the loops remain essentially intact after interaction with the dislocation, except being partially absorbed and sheared. This effect, too, may have consequences regarding the strain hardening evolution and in particular, the formation of defect-free channels, expected to be prevented or at least delayed.

Acknowledgements

Part of the calculations were performed at HPC Julich. The work was partially supported by the EURATOM Seventh Framework Programme, under the Perform60 project and for the rest by the SCK·CEN project MENPHIS. It contributes to the Joint Programme on Nuclear Materials of the European Energy Research Alliance. Xinfu HE acknowledges National Basic Research Program of China, Grant Number 2011CB610503 and National Natural Science Foundation of China, Grant Number 51201184 and 11375270.

References

[1] G.R. Odette, Scr. Metall. 17 (1983) 1183.
[2] G.R. Odette, G.E. Lucas, J. Miner. Met. Mater. Soc. 53 (2001) 18.
[3] G.R. Odette, C.L. Liu, B.D. Wirth, Microstructure Evolution During Irradiation, vol. 439, 1997, p. 457.
[4] C.A. English, W.J. Phythian, R.J. McElroy, Microstructure Evolution During Irradiation, vol. 439, 1997, p. 471.
[5] G.R. Odette, R.K. Nanstad, JOM 61 (2009) 17.
[6] G. Bonny, D. Terentyev, A. Bakaev, E.E. Zhurkin, M. Hou, D. Van Neck, L. Malerba, J. Nucl. Mater. 442 (2013) 282.
[7] E. Meslin et al., J. Nucl. Mater. 406 (2010) 73.
[8] G. Bonny, D. Terentyev, E.E. Zhurkin, L. Malerba, J. Nucl. Mater. 452 (2014) 486–492.
[9] S.C. Glade, B.D. Wirht, G.R. Odettes, P. Asoka-Kumar, P.A. Sterne, R.H. Howell, Philos. Mag. 85 (2003) 629.
[10] M. Lambrecht, L. Malerba, A. Almazouzi, J. Nucl. Mater. 378 (2008) 282.
[11] Y. Nagai, K. Takadate, Z. Tang, H. Ohkubo, H. Sunaga, H. Takizawa, M. Hasegawa, Phys. Rev. B 67 (2003) 224202.
[12] D. Terentyev, L. Malerba, G. Bonny, A.T. Al-Motasem, M. Posselt, J. Nucl. Mater. 419 (2011) 134.
[13] D. Terentyev, L. Malerba, J. Nucl. Mater. 421 (2012) 32.
[14] J. Kocik, E. Kielova, J. Cizek, I. Prochazka, J. Nucl. Mater. 303 (2002) 52.
[15] G. Maussner, L. Scharf, R. Langer, B. Gurovich, Nucl. Eng. Des. 193 (1999) 359.
[16] E.A. Kuleshova, B.A. Gurovich, Y.I. Shtrombakh, D.Y. Erak, O.V. Lavrenchuk, J. Nucl. Mater. 300 (2002) 127.
[17] B.A. Gurovich, E.A. Kuleshova, Y.I. Shtrombakh, D.Y. Erak, A.A. Chernobaeva, O.O. Zabusov, J. Nucl. Mater. 389 (2009) 490.

[18] K. Fukuya, K. Ohno, H. Nakata, S. Dumbill, J.M. Hyde, J. Nucl. Mater. 312 (2003) 163.
[19] M. Hernandez-Mayoral, D. Gomez-Briceno, J. Nucl. Mater. 399 (2010) 146.
[20] K. Fujii, K. Fukuya, N. Nakata, K. Hono, Y. Nagai, M. Hasegawa, J. Nucl. Mater. 340 (2005) 247.
[21] T. Hamaoka, Y. Satoh, H. Matsui, J. Nucl. Mater. 399 (2010) 26.
[22] D.T. Hoelzer, F. Ebrahimi, Mat. Res. Soc. Symp. Proc. 373 (1995) 57.
[23] A. Okada, H. Maeda, K. Hamada, I. Ishida, J. Nucl. Mater. 271&272 (1999) 133.
[24] A. Calder, D. Bacon, J. Nucl. Mater. 207 (1993) 25.
[25] L. Malerba, J. Nucl. Mater. 351 (2006) 28.
[26] D. Terentyev, C. Lagerstedt, P. Olsson, K. Nordlund, J. Wallenius, C. Becquart, L. Malerba, J. Nucl. Mater. 351 (2006) 65.
[27] P. Olsson, T.P.C. Klaver, C. Domain, Phys. Rev. B 81 (2010) 054102.
[28] M. Mendelev, S. Han, D. Srolovitz, Philos. Mag. 83 (2003) 3977.
[29] A. Voter, S. Chen, Mater. Res. Soc. Symp. Proc. 82 (1987) 175.
[30] Y. Mishin, M. Mehl, D. Papaconstantapoulos, Phys. Rev. B 63 (2001) 224106.
[31] G. Bonny, R.C. Pasianot, N. Castin, L. Malerba, Philos. Mag. 89 (2009) 3531.
[32] G. Bonny, R.C. Pasianot, L. Malerba, Modell. Simul. Mater. Sci. Eng. 17 (2009) 025010.
[33] R. Pasianot, L. Malerba, J. Nucl. Mater. 360 (2007) 118.
[34] M. Allen, D. Tildesley, Computer Simulation of Liquids, Clarendon Press, Oxford, 1987.
[35] D. Terentyev, N. Anento, A. Serra, J. Phys. – Condens. Matter 24 (2012) 455402.
[36] Y.N. Osetsky, D.J. Bacon, Modell. Simul. Mater. Sci. Eng. 11 (2003) 427.
[37] D. Hull, D.J. Bacon, Introduction to dislocations, Butterworth-Heinemann, Oxford, 2001.
[38] D. Bacon, Y. Osetsky, Z. Rong, Philos. Mag. 86 (2006) 3921.
[39] D. Terentyev, D. Bacon, Y. Osetsky, J. Phys.: Condens. Matter 20 (2008) 445007.
[40] D. Terentyev, D.J. Bacon, Y.N. Osetsky, Philos. Mag. 90 (2010) 1019.
[41] D. Terentyev, L. Malerba, D. Bacon, Y. Osetsky, J. Phys.: Condens. Matter 19 (2007) 456211.
[42] D. Terentyev, P. Grammatikopoulos, D. Bacon, Y. Osetsky, Acta Mater. 56 (2008) 5034.
[43] Z. Rong, Y.N. Osetsky, D.J. Bacon, Philos. Mag. 85 (2005) 1473.
[44] D. Terentyev, A. Bakaev, J. Phys. – Condens. Matter 25 (2013) 265702.
[45] A. Nomoto, N. Soneda, A. Takahashi, S. Ishino, Mater. Trans. 46 (2005) 463.
[46] D.A. Terentyev, Y.N. Osetsky, D.J. Bacon, Acta Mater. 58 (2010) 2477.
[47] E.E. Zhurkin, D. Terentyev, M. Hou, L. Malerba, G. Bonny, J. Nucl. Mater. 417 (2011) 1082.
[48] D. Terentyev, N. Anento, A. Serra, J. Nucl. Mater. 420 (2012) 9.
[49] A. Bakaev, D. Terentyev, G. Bonny, T.P.C. Klaver, P. Olsson, D. Van Neck, J. Nucl. Mater. 444 (2014) 237.